IOP PUBLISHING PLASMA PHYSICS AND CONTROLLED FUSION

Plasma Phys. Control. Fusion **52** (2010) 095009 (15pp) doi:10.1088/0741-3335/52/9/095009

Numerical simulation on edge localized mode control capability of resonant magnetic perturbation in the KSTAR tokamak

Doohyun Kim[1], Hyunsun Han[1], Ki Min Kim[1], Jong Kyu Park[2], Young Mu Jeon[3], Yong-Su Na[1] and Sang Hee Hong[1]

[1] Department of Nuclear Engineering, Seoul National University, Seoul 151-742, Korea
[2] Princeton Plasma Physics Laboratory, Princeton, NJ 08543, USA
[3] National Fusion Research Institute, Daejeon 305-333, Korea

E-mail: hongsh@snu.ac.kr

Received 12 May 2010, in final form 12 July 2010
Published 13 August 2010
Online at stacks.iop.org/PPCF/52/095009

Abstract

Numerical simulations are carried out to investigate the applicability of resonant magnetic perturbation (RMP) to KSTAR plasmas for a possible control of edge localized mode (ELM) to suppress or mitigate its damages to divertor materials. For the verification of the feasibility of RMP application, magnetic island configurations, resonant normal fields, magnetic island widths and Chirikov parameters are calculated for two types of KSTAR operation scenarios: steady state and hybrid. Field error correction (FEC) coils in KSTAR are considered to produce externally perturbed magnetic fields for RMP, and the directions of coil currents determine the toroidal mode n and the parity (even or odd). The RMP configurations are described by vacuum superposition of the equilibrium magnetic fields and the perturbed ones induced by FEC coils. The numerical simulations for $n = 2$ toroidal mode in both operation scenarios show that when the pitches of the equilibrium and perturbed magnetic fields are well aligned, magnetic islands are formed for a series of m poloidal modes and the adjacent islands are overlapped to generate a stochastic layer in the edge region. Even parity turns out to be more effective in making the magnetic islands overlapped to become stochastic field lines in the steady-state operation, while odd parity in the hybrid operation. The formation of the stochastic layer is verified by the calculated Chirikov parameters, which also give basic information on the current requirement of FEC coils. Additionally, lobe structures of stochastic field lines are found in the edge region extended to the divertor plate in the hybrid scenario. Based on the standard vacuum criteria for RMP, the simulation results indicate that the FEC coils will be feasible for control of ELMs and mitigation of divertor heat load by RMP in both steady-state and hybrid operation scenarios.

(Some figures in this article are in colour only in the electronic version)

1. Introduction

Future tokamak fusion devices, such as ITER and DEMO, aim at long-pulse operations with high performance, i.e. the so-called advanced tokamak (AT) operation mode [1]. To achieve this goal, tokamak fusion plasmas should be sustained in a controlled way for a long time, and plasma facing components (PFCs) have to bear the burden of heavy particle fluxes and high heat loads from core plasmas. Edge localized mode (ELM) is one of the main sources that make the plasma confinement deteriorate and yield endurable loads of particles and heat to PFCs [2] like divertor plates. The ELM leads to repeated decays in the density and temperature of the plasma in the pedestal region and, in particular, Type I ELM can cause the durability of the divertor material to be shortened by delivering intense heat loads repetitively onto the divertor plate. Therefore, the ELM should be controlled to achieve the AT operation in ITER or DEMO. There are several ways to control or mitigate ELM and ELM energy loss to the divertor plate, such as intended ELM triggering by pellet injection [3], impurity injection [4] and edge current modification [5]. Among them, resonant magnetic perturbation (RMP) is expected to be one of the most efficient ways for ELM control without a critical degeneration of plasma confinement [6].

Generally, RMP can reduce the amplitudes of ELM fluctuations by increasing the ELM frequency and thus suppress the ELM heat load to the divertor considerably. On the other hand, RMP can trigger ELMs in an ELM-free discharge [7]. In addition, RMP is able to give rise to the extension of divertor lifetime. Small non-axisymmetric magnetic perturbations transform the axisymmetric separatrix to helical invariant manifolds, which are called 'homoclinic tangles' [8]. These magnetic field structures can bring about the split of divertor strike point to reduce the deposition of peak heat and particle fluxes onto the divertor plate [9].

Even though research on RMP has been actively conducted, the physics of RMP is not yet clearly disclosed, and quantitative requirements of RMP strength and spectra are still under investigation. Recently, four guidelines called vacuum criteria have been suggested for RMP studies on ELM suppression [7]. Firstly, the external coils for RMP should be placed as close as possible to the plasma to generate maximal edge perturbations, but minimal core perturbations. Secondly, the rows of coil arrangement should be set both above and below the mid-plane on the outboard side. The third one is the pitch alignment between the equilibrium and external magnetic fields induced by the RMP coils. If the pitches of the two magnetic fields are well harmonized, the RMP can be effective in ELM control. The last criterion is the Chirikov condition that reveals the level of overlap between two adjacent islands. If the Chirikov parameter is greater than unity, the overlap of magnetic islands is ensured, in other words, the generation of a stochastic layer. If a stochastic layer is generated in an appropriate region, usually near the position of the top of pedestal, ELMs can be suppressed. These criteria are based on vacuum field calculations in the absence of plasma responses or shielding effect by rotation. The ITER also deliberates on constructing RMP coils for ELM control, of which capability and design are being estimated with the vacuum criteria described above [10].

The generation of a stochastic layer near the pedestal region may be a prerequisite for ELM suppression, but it is not a sufficient condition. Although the simulation results on MAST and NSTX showed that Chirikov parameters were greater than unity near the pedestal top region and the stochastic layers were formed around the pedestal region, ELMs were not suppressed in the real experiments on these spherical tori [11, 12]. The criterion based on Chirikov parameter value (>1) near the pedestal top does not seem to work well either in other tokamaks including JET [13]. However, the Chirikov parameter could provide basic information and be considered as an RMP criterion in the early steps for the study of its applicability to ELM suppression.

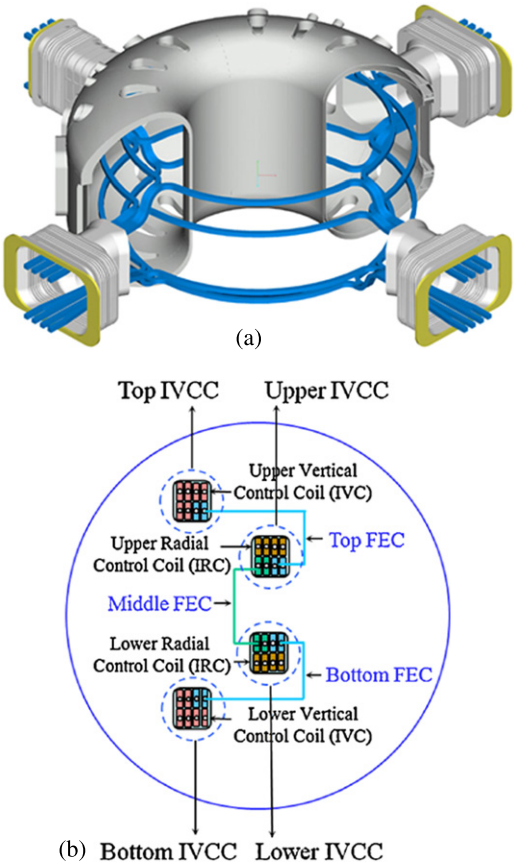

Figure 1. Configurations of the KSTAR IVCCs: (*a*) a 3D view installed inside the vacuum vessel and (*b*) a cross sectional view of four coil segments (top, upper, lower and bottom) intersected by a half-plane with the major axis as an edge. Each coil segment has different functions of fast vertical and radial position control, error field correction and RWM control. The whole IVCC assembly consists of two sets of four closed coil loops in the shape of a quarter-circular ribbon along the toroidal direction with up–down symmetry about the mid-plane [15].

The KSTAR (Korea Superconducting Tokamak Advanced Research) tokamak [14] is planned to be equipped with an in-vessel control coil (IVCC) system [15] which has a picture-framed structure with external connection circuits to provide multi-purpose control capabilities. The KSTAR IVCC system, which is illustrated in figure 1, has been designed to be capable of achieving the control of vertical and radial plasma positions, field error correction (FEC) and resistive wall mode (RWM) stabilization. Since the main goal of KSTAR experiments is long-pulse operations of high performance plasmas such as AT scenarios [1], the application of RMP is essential to suppress ELMs for extending the divertor lifetime in the long-pulse duration of up to 300 s. Even though the pedestal pressure and the energy deposition density during ELMs are yet to be quantitatively analyzed in detail for KSTAR, the potential damage on the divertor plates due to large ELMs may become a serious problem during the planned AT operations. Moreover, under the current situation that ITER considers to employ the RMP for ELM control, the RMP capability in KSTAR as a pilot device for ITER should be examined in advance. This numerical work will make an attempt to verify the RMP capability of ELM

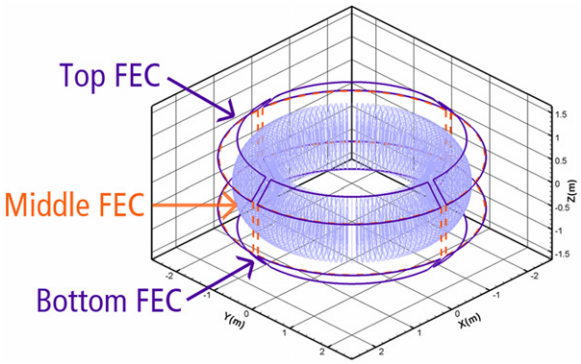

Figure 2. Schematic view of the FEC coils among the IVCCs in KSTAR. Only top and bottom FEC control coils are considered in this numerical work for RMP analysis. The direction of current in each coil determines the toroidal mode number and the parity (even or odd) under a fixed current of 10 kA flowing in each coil.

suppression by using the FEC coils in the KSTAR IVCC system and to provide basic technical information, such as engineering limit of the FEC power supply.

This paper is organized as follows: the theoretical formulation and numerical approach employed in this work are described in section 2, including target of calculation, computational scheme. Section 3 presents the simulation results and discussion on the RMP for the steady-state and hybrid operation scenarios of the KSTAR tokamak, respectively. Finally, section 4 presents the conclusion.

2. Theoretical and numerical formulation

The KSTAR IVCC assembly, shown in figure 1, is composed of three types of control coils for in-vessel vertical control (IVC), in-vessel radial control (IRC) and FEC. The upper and lower IVC and IRC coils have been designed for the fast control of plasma positions with an anti-series connection for IVC and a series connection for IRC. The up–down symmetric FEC coils have been designed to have picture-framed structures for multi-purpose controls, such as FEC control, ELM control by RMP and RWM control. KSTAR has three FEC coils (top, bottom and middle) crossed on the poloidal plane and four FEC coils placed 90° apart along the toroidal direction. Hence, totally 12 FEC coils are available.

Figure 2 shows a schematic view of the structure and arrangement of the FEC coils considered in this simulation work. Since the middle FEC coils drawn in dashed lines are wholly designated for RWM control, the top and bottom FEC coils shown in solid lines are employed to investigate the RMP capability on KSTAR plasmas. It is assumed that a dc current of 10 kA is flowing through each coil and the direction of current is changeable individually. The currents on each coil induce perturbed magnetic fields superposed on the vacuum equilibrium fields, and the direction of current brings about various types of toroidal field harmonics in the resultant magnetic field configuration. The combination of current directions in the upper and lower coil sets determines the parity of the field configuration as well. In the case of up–down symmetry, which implies that the directions of currents in the upper and lower coil sets are the same, the corresponding field configuration is designated as even parity, while the opposite case, up–down asymmetry, is called odd parity [9]. In this numerical simulation, the directions of coil currents are designed to favorably form the $n = 2$ toroidal mode, and both even and odd parities are taken into account.

A perturbed magnetic field configuration can be obtained by adding the external magnetic fields generated by FEC coils to the equilibrium magnetic fields. The poloidal equilibrium magnetic field, which has radial and axial components, B_R and B_Z, in cylindrical coordinates (R, Z, ϕ), is calculated using the poloidal magnetic flux function ψ obtained from the Grad–Shafranov equation, and the toroidal field B_ϕ is determined from the poloidal current flux $F(\psi)$ [16]. The external fields induced by coil currents I are calculated using the Biot–Savart law [17]. To find the magnetic field configuration, a vacuum superposition of the equilibrium and external magnetic fields is only considered by neglecting the effects of plasma responses, such as rotational shielding and self-consistent perturbed magnetic fields in the plasma. A field line tracing code has been developed in this work for visualizing the magnetic field configuration. The poloidal positions of magnetic field lines are found in this code along the increment of a step size in the toroidal direction, and the resultant magnetic field configurations are illustrated in the form of Poincaré plots.

For a qualitative estimation of the degree of resonance between equilibrium and external magnetic fields, resonant normal magnetic fields $\tilde{B}_\mathrm{r}$ are analyzed by the Fourier superposition principle. The Fourier analyzed resonant normal fields $\tilde{B}_{\mathrm{r}(m,n)}$ can be derived in the same way as Fourier decomposition of non-axisymmetric poloidal flux $\tilde{\psi}_\mathrm{p}$ in magnetic coordinates (ψ, θ, ϕ) [18]. The two-dimensional Fourier analyzed $\tilde{\psi}_\mathrm{p}$ in poloidal and toroidal harmonics can be written as

$$\tilde{\psi}_\mathrm{p}(\theta, \phi) = \frac{\tilde{\psi}_{0,0}}{2} + \sum_{\substack{-\infty < m < \infty \\ 0 < n < \infty}} [\tilde{\psi}_{\mathrm{c},m,n} \cos\alpha_{m,n} + \tilde{\psi}_{\mathrm{s},m,n} \sin\alpha_{m,n}], \tag{1}$$

$$\tilde{\psi}_{\mathrm{c},m,n} = \frac{1}{(2\pi)^2} \int_0^{2\pi} \int_0^{2\pi} 2\tilde{\psi}_\mathrm{p} \cos\alpha_{m,n} \,\mathrm{d}\theta \,\mathrm{d}\phi, \tag{2}$$

$$\tilde{\psi}_{\mathrm{s},m,n} = \frac{1}{(2\pi)^2} \int_0^{2\pi} \int_0^{2\pi} 2\tilde{\psi}_\mathrm{p} \sin\alpha_{m,n} \,\mathrm{d}\theta \,\mathrm{d}\phi, \tag{3}$$

where $\alpha_{m,n} = m\theta - n(\phi - \phi_0)$, and m and n are the poloidal and toroidal mode numbers, respectively. The cosine and sine terms of Fourier harmonic amplitudes of $\tilde{B}_{\mathrm{r}(m,n)}$ can be obtained in a similar way:

$$\tilde{B}_{\mathrm{c,r}(m,n)} \equiv \frac{\iint 2J\tilde{B}_\mathrm{r} \cos\alpha_{m,n} \,\mathrm{d}\theta \,\mathrm{d}\phi}{\iint J \,\mathrm{d}\theta \,\mathrm{d}\phi}, \qquad \tilde{B}_{\mathrm{s,r}(m,n)} \equiv \frac{\iint 2J\tilde{B}_\mathrm{r} \sin\alpha_{m,n} \,\mathrm{d}\theta \,\mathrm{d}\phi}{\iint J \,\mathrm{d}\theta \,\mathrm{d}\phi}, \tag{4}$$

where $J = (q/R_0B_0)R^3B_\theta$ is the Jacobian of magnetic coordinates, q is the safety factor, R_0 is the major radius, B_0 is the vacuum toroidal magnetic field, B_θ is the poloidal magnetic field and $\iint J \,\mathrm{d}\theta \,\mathrm{d}\phi$ is the surface area S of each rational surface. With these two harmonic amplitudes, the physical harmonic amplitude of resonant normal fields for (m, n) modes can be obtained as

$$\tilde{B}_{\mathrm{r}(m,n)} = \sqrt{\tilde{B}^2_{\mathrm{c,r}(m,n)} + \tilde{B}^2_{\mathrm{s,r}(m,n)}}. \tag{5}$$

Since the area element $J \,\mathrm{d}\theta \,\mathrm{d}\phi$ has an invariant value independent of the coordinate system, the resonant Fourier harmonics are the same in all magnetic coordinates if $m = nq$ [19]. This means that although the magnetic field configuration depends on the distortion of toroidal angle along the change of coordinates, the resonant normal fields are regardless of the choice of the coordinate system.

Table 1. Plasma parameters for the steady-state and hybrid operation scenarios of KSTAR. As the operation phase I, the steady-state operation scenario will conduct the experiments at high β_N with relatively low B_{T0} and I_P. The hybrid operation scenario aims at higher β_N with elevated B_{T0} and I_P in the operation phase II.

Operation mode	β_N	q_{95}	B_{T0} (T)	I_P (MA)	l_i	R_0 (m)	a (m)
Steady state	3.0	5.3	2.0	1.0	0.4	1.8	0.5
Hybrid	3.5	3.8	3.5	2.0	1.0	1.8	0.5

The generation of a stochastic layer is verified quantitatively by calculating the widths of magnetic islands. The magnetic island width w_p for (m, n) modes is related to the physical harmonic amplitude of Fourier analyzed poloidal flux $\tilde{\psi}_{m,n}$ as follows [18]:

$$w_p = \sqrt{16\frac{q}{q'}\tilde{\psi}_{m,n}}, \tag{6}$$

where $q' = dq(\psi_p)/d\psi_p$. The Fourier analyzed poloidal flux $\tilde{\psi}_{m,n}$ is related to the physical harmonic amplitude $\tilde{B}_{r(m,n)}$ as

$$\tilde{\psi}_{m,n} = \frac{S}{(2\pi)^2 m}\tilde{B}_{r(m,n)}. \tag{7}$$

Combining these relations, the width of magnetic islands in equation (6) can be rewritten in terms of the normalized poloidal flux ψ_N as

$$w_{pN} = \sqrt{\frac{16}{m\,|\Delta\psi_p|}\frac{q}{dq(\psi_N)/d\psi_N}\frac{S}{(2\pi)^2}\tilde{B}_{r(m,n)}}, \tag{8}$$

where $\Delta\psi_p$ is the difference between the poloidal flux functions at the magnetic axis and at the plasma boundary. The width of a magnetic island centered on a rational surface is calculated by the resonant normal fields to determine the Chirikov parameter.

The Chirikov parameter obtained from the widths of islands indicates the degree of overlap between two adjacent islands, and judges whether a stochastic layer is generated or not. The Chirikov parameter can be written as [18]

$$C_{(m,n)} = \frac{0.5(w_{pN,m+1} + w_{pN,m})}{\psi_{N(m+1,n)} - \psi_{N(m,n)}}. \tag{9}$$

If the Chirikov parameter is greater than unity, two adjacent magnetic islands are overlapped so that a stochastic layer is formed. The Chirikov parameter defined in equation (9) is considered as a metric for the measurement of the overlap of magnetic islands.

In this work, a numerical code, named 'RAFT' (RMP Analysis and Fieldline Tracing), has been developed using the algorithms of 'TRIP3D' [20] and 'SURFMN' [18] codes, respectively, for visualizing the magnetic island configurations and calculating resonant normal fields, magnetic island widths and Chirikov parameters in the two types of KSTAR operation scenarios.

3. Simulation results and discussion

In this numerical simulation, two types of KSTAR operation scenarios are employed. One is an ITER relevant steady-state operation scenario [1] in the KSTAR operation phase I, and the other is a hybrid operation scenario [21] in the KSTAR operation phase II. The plasma parameters for each scenario are listed in table 1. To achieve a high normalized beta β_N of

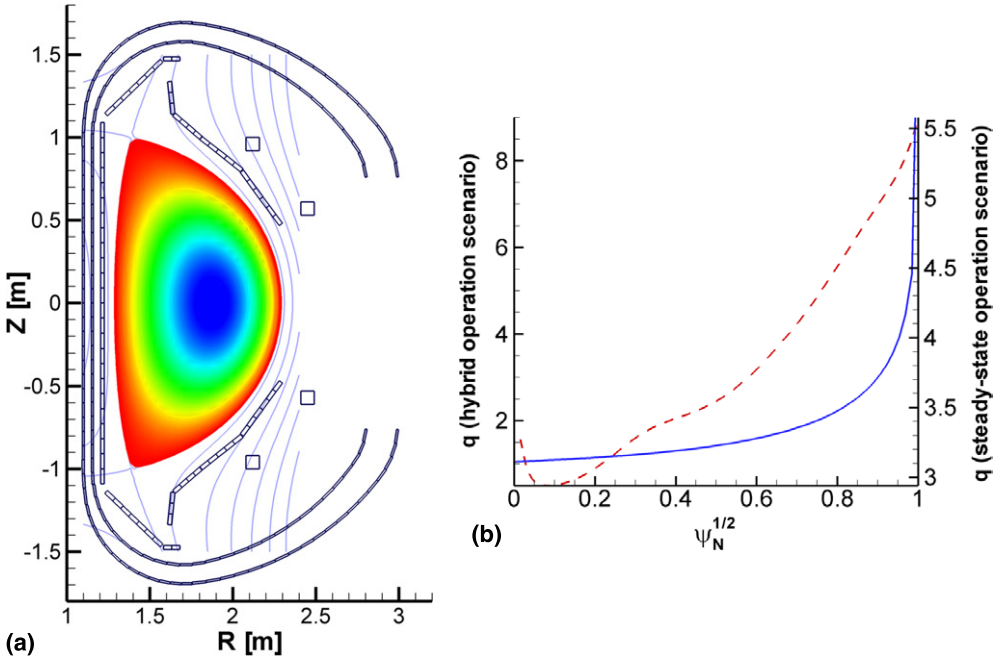

Figure 3. (*a*) Poloidal flux surface configuration and (*b*) radial profile of q-values of the equilibrium plasma in the KSTAR steady-state (dashed) and hybrid (solid) operation scenarios.

about 3.0 with a limited heating power in the steady-state operation scenario, the vacuum toroidal magnetic field B_{T0} and plasma current I_P have been set to be lower than their goal in the KSTAR final operation phase. In the hybrid operation phase, KSTAR is expected to achieve a higher normalized beta β_N of 3.5 at 3.5 T of B_{T0} and 2.0 MA of I_P.

Typically, figure 3(*a*) shows the magnetic flux surface configuration of the free-boundary equilibrium plasma for the hybrid operation scenario. In figure 3(*b*), the dashed and solid curves indicate the q-profiles of the equilibrium plasmas for the steady-state and hybrid operation scenarios, respectively. The q-profile of the steady-state operation having $q_{95} \sim 5.3$ is strongly reversed near the center due to the lack of central current drive. Here, a balanced neutral beam injection (NBI) using two beam sources is applied to result in nearly zero neutral beam current drive (NBCD). Additionally, lower hybrid current drive (LHCD) at 5 GHz is used for an off-axis current drive [1]. Unlike the steady-state operation scenario, the q-profile of the hybrid operation scenario maintains a flat shape with slightly greater values than unity around the center region and has a steep gradient near the edge region. The value of q_{95} is about 3.8 which is smaller than that in the steady-state case.

To investigate the applicability of RMP to each operation scenario, magnetic island configurations and widths, resonant normal fields and Chirikov parameters are examined by following the ways and procedures described in section 2.

3.1. Steady-state operation scenario

When the perturbed magnetic fields induced by FEC coils in KSTAR are superposed on the equilibrium fields, a variety of magnetic islands are generated depending on the poloidal and toroidal mode numbers (m, n) and the parity of the FEC coil currents. The magnetic island

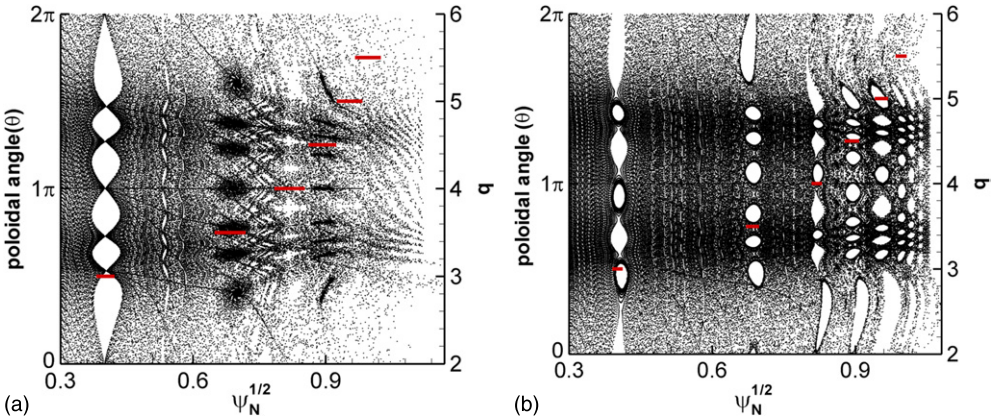

Figure 4. Cutaway view of magnetic island configurations and the calculated island widths (a) for even parity and (b) for odd parity of the $n = 2$ mode in the KSTAR steady-state operation scenario. The magnetic island widths for even parity are wider than the corresponding ones for odd parity. The stochastic trajectories of magnetic field lines appear outside the $q = 9/2$ rational surface for even parity, whereas they do not appear in the whole region for odd parity.

configurations and widths of the $n = 2$ toroidal mode are presented in figure 4 for even and odd parities, respectively. The vertical and horizontal axes represent the poloidal angle θ and the radial position $\psi_N^{1/2}$, respectively. The magnetic islands are formed for both parities around the rational surfaces satisfying that $q(\psi_N^{1/2}) = m/n$, and their sizes appear to be nearly matched with the calculated widths that are indicated by horizontal thick bars at the corresponding q positions, respectively. In the case of even parity, the island widths are larger than those for odd parity. For the $q = m/n = 9/2$ surface, the size of the magnetic islands seems to be smaller than the calculated island width. This comes from the overlap of the magnetic islands in this region, and the stochastic trajectories of the magnetic field lines start appearing near this surface. The magnetic islands are fully overlapped from the $q = 10/2$ surface so that they are practically invisible in figure 4(a) due to the stochasticity of field lines. The stochastic layer generation has resulted from the overlap of the magnetic islands in this region. On the other hand, in the case of odd parity, all the magnetic islands turn out to be not overlapped in the whole region and maintain their island shapes and widths on the corresponding rational surfaces, as shown in figure 4(b).

As the poloidal mode numbers are scanned from $m = -30$ to $m = 30$, the resonant normal fields $\tilde{B}_{r(m,n)}$ are varied according to the parity of the FEC coil currents as appearing in figure 5 at a fixed toroidal mode number of $n = 2$. The dashed curves in this figure indicate all the rational surfaces of equilibrium magnetic fields. Figure 5(a) for even parity shows the resonant normal field distribution depending on m. There are two ridges in this $\tilde{B}_{r(m,n=2)}$ contour plot: the first ridge near $m = 1$ is narrow while the second one with broader spectra of m is located in the higher m region. In this case, the second ridge of resonant normal fields matches well with the equilibrium fields on the rational surfaces in the edge region. This means that the externally perturbed fields intensively resonate with the equilibrium fields near rational surfaces, and such resonances generate magnetic islands to expand their sizes to overlap with one another near the edge region. On the other hand, in figure 5(b) for odd parity, the pitches of the resonant normal fields do not match with those of the equilibrium fields, and thus the resonance between the two fields does not occur sufficiently to make the magnetic islands as large as those for even parity. Such pitch matching between the equilibrium and externally

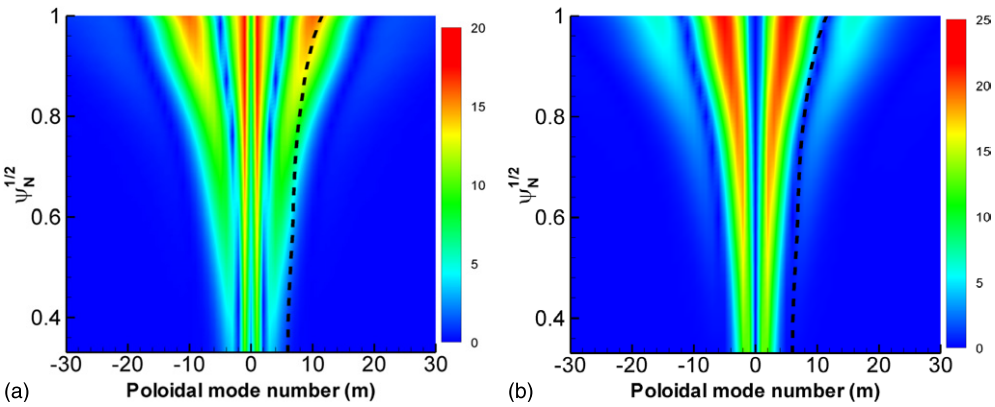

Figure 5. Contour plots of resonant normal field $\tilde{B}_{r(m,2)}$ in gauss unit (a) for even parity and (b) for odd parity of the $n = 2$ mode in the KSTAR steady-state operation scenario. The dashed curve indicates the $q = m/2$ surfaces showing the locus of pitch resonance. In the steady-state operation scenario, the pitch alignments are better for even parity than those for odd parity.

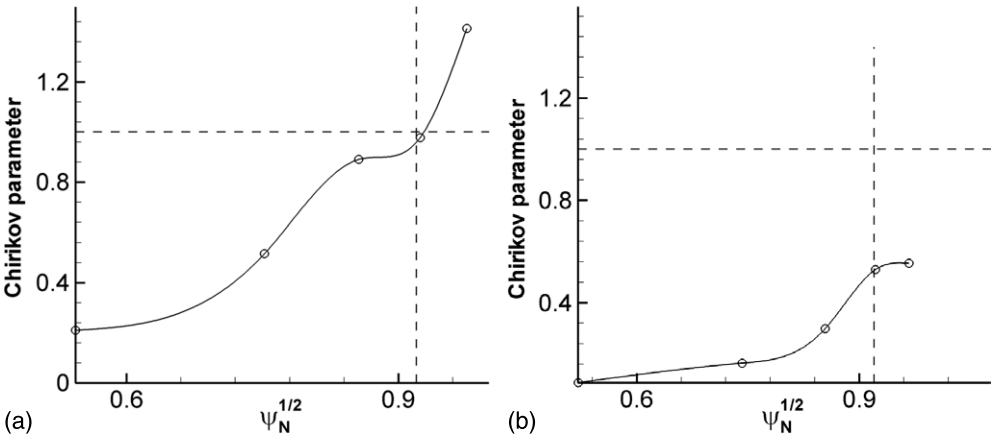

Figure 6. Chirikov parameters (a) for even parity and (b) for odd parity of the $n = 2$ mode in the KSTAR steady-state operation scenario. In the even parity case, the Chirikov parameters are greater than unity in the edge region beyond the pedestal top position at $\psi_N^{1/2} \sim 0.92$, which indicates that the overlapped islands form a stochastic layer. On the other hand, in the odd parity case, all the Chirikov parameters are smaller than unity in the whole plasma region, which means no stochastic layer is formed.

induced magnetic fields could well explain the formation of magnetic islands for both parities seen in figure 4.

The overlap of magnetic islands is quantitatively judged by the estimated Chirikov parameters, of which profiles are shown in figure 6 for both parities of the $n = 2$ mode. The vertical dashed lines point out the position of the pedestal top at $\psi_N^{1/2} \sim 0.92$, which satisfy the vacuum criteria in the steady-state operation scenario. In even parity, the Chirikov parameters are greater than unity in the edge region beyond $\psi_N^{1/2} \sim 0.928$. This implies that a stochastic layer is generated by the overlap of magnetic islands around the pedestal. The Chirikov parameters for odd parity shown in figure 6(b) appear to be lower than unity in the

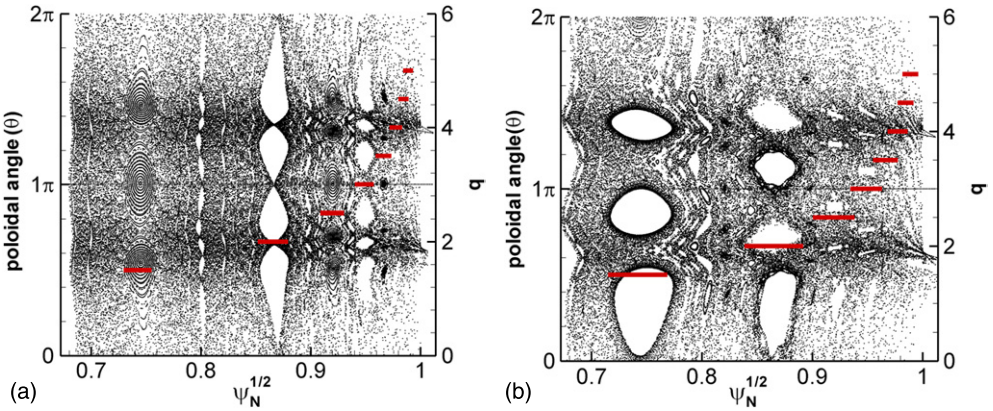

Figure 7. Cutaway view of magnetic island configurations and the calculated island widths (*a*) for even parity and (*b*) for odd parity of the $n = 2$ mode in the KSTAR hybrid operation scenario. The sizes of magnetic islands for odd parity are larger than those of the corresponding ones for even parity. The stochastic trajectories of magnetic field lines appear beyond $q = m/n = 7/2$ and $5/2$ rational surfaces in the edge region for even and odd parities, respectively.

whole region where stochastic layers are not created, and thus the RMP criterion is not satisfied in the odd parity case.

Additionally, the optimal FEC coil currents can be determined by the Chirikov parameter, since the parameter is proportional to the square root of FEC coil currents according to the relationship among Chirikov parameter, island width, resonant field amplitude and the current. In the even parity, the Chirikov parameter at $\psi_N^{1/2} \sim 0.92$ is about 0.96 which resulted from 10 kA of FEC coil current. According to the RMP criterion, the required current is estimated to be 12 kA of each coil current to form a stochastic layer near the pedestal top. Similarly, about 36 kA will be needed for odd parity.

3.2. Hybrid operation scenario

In a similar way to the steady-state case, magnetic island configurations and sizes, resonant normal fields and Chirikov parameters are calculated for the hybrid operation scenario. In addition, the lobe structure of the perturbed magnetic field lines extended to the divertor region is examined to confirm the stochasticity of magnetic field lines.

The magnetic island configurations and widths resulted from the even and odd parities of the $n = 2$ mode by FEC coil currents are illustrated in figure 7 for the hybrid operation scenario. In figure 7(*a*) for even parity, the magnetic islands maintain their shapes up to the $q = m/n = 6/2$ surface, and start overlapping near the $q = 7/2$ surface to end with stochastic trajectories of magnetic field in the edge region. Overlapping of the magnetic islands beyond the $q = 7/2$ surface can be easily seen from doubling of the calculated widths of the adjacent magnetic islands in this region. As shown in figure 7(*b*), the magnetic islands for odd parity appear larger than those for even parity. The islands start to overlap and the stochastic field lines appear from the $q = m/n = 5/2$ surface to be fully developed beyond the $q = 6/2$ surface. Unlike the steady-state operation scenario, both even and odd parities show the overlap of magnetic islands and the resultant stochastic trajectories near the edge region, which is qualitative evidence of the stochastic layer generation. However, the magnetic field lines seem to be more stochastic in the odd parity case, compared with those in the even parity case.

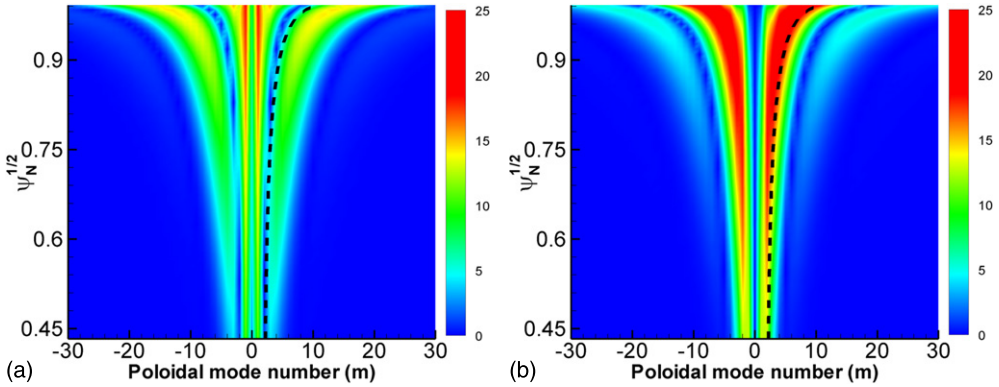

Figure 8. Contour plots of resonant normal field $\tilde{B}_{r(m,2)}$ in gauss unit (a) for even parity and (b) for odd parity of the $n = 2$ mode in the KSTAR hybrid operation scenario. The dashed curve indicates the $q = m/2$ surfaces showing the locus of pitch resonance. Contrary to the steady-state operation scenario, the pitch alignments are better for odd parity than those for even parity in the hybrid operation scenario.

The calculation results of Fourier analyzed resonant normal fields for the hybrid operation scenario are exhibited in figure 8. In the contour plots for even parity shown in figure 8(a), the dashed lines for the equilibrium fields are close to the second ridge of the resonant fields but not aligned well. Although the pitches of the two fields are not completely matched, they would be somewhat resonant to make the magnetic islands overlap in the edge region. This resonance brings about the overlap of magnetic islands outside the $q = 7/2$ surface as seen in figure 7(a). The resonance between the equilibrium and resonant normal fields for odd parity turns out to be apparent as seen in figure 8(b), in which the pitches of the two fields are well aligned. Similarly to the even parity of the steady-state scenario, the two fields are strongly resonant with each other to generate large magnetic islands that form a stochastic layer. The degrees of how the two magnetic fields are resonant for both parities reasonably explain the formation of the corresponding magnetic island configurations shown in figure 7. As the two fields are strongly resonant, the widths of the islands become larger and the stochastic layer is formed near the edge plasma region.

The overlap of magnetic islands and the generation of stochastic layer are quantitatively verified by Chirikov parameters presented in figures 9(a) and (b) for even and odd parities, respectively. In both figures, the vertical dashed lines indicate the position of the pedestal top assumed at $\psi_N^{1/2} \sim 0.92$ as in the steady-state scenario. In figure 9(a) for even parity, the Chirikov parameters are greater than unity near $\psi_N^{1/2} \sim 0.964$, where the islands are overlapped to produce a stochastic layer. Although the stochastic layer is created, the RMP criterion is not satisfied since its location is distant from the position of the pedestal top. The Chirikov parameters for odd parity shown in figure 9(b) are greater than unity near $\psi_N^{1/2} \sim 0.917$, which is close to the pedestal top position where the overlap of magnetic islands and the formation of stochastic layer should take place for ELM suppression. Therefore, the odd parity case satisfies the RMP criteria more favorably than the even parity case.

Furthermore, the optimal FEC coil currents are calculated using the Chirikov parameter. In the odd parity case driven with 10 kA of FEC coil current, a stochastic layer is formed at the top of the pedestal at $\psi_N^{1/2} \sim 0.92$ where the Chirikov parameter turns out to be 1.02. On the other hand, about 31 kA is needed for even parity to satisfy the RMP criteria for ELM

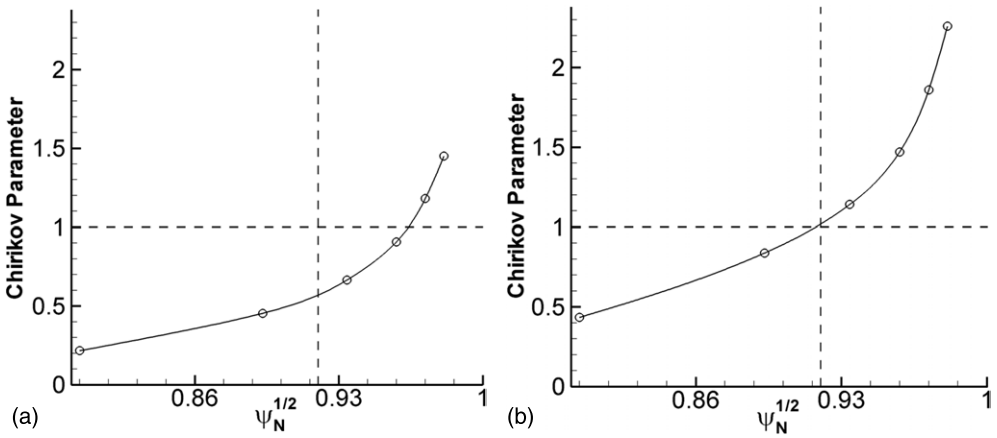

Figure 9. Chirikov parameters (*a*) for even parity and (*b*) for odd parity of the $n = 2$ mode in the KSTAR hybrid operation scenario. In the case of odd parity, the Chirikov parameters are larger than unity in the edge region, and thus the overlapped islands form a stochastic layer. Although the magnetic islands are overlapped for even parity as well, the stochastic layer is formed far away from the edge pedestal position.

suppression. These results can give the useful basic information for KSTAR operation in the future.

The magnetic perturbation generated by FEC coils brings about a transformation of the unperturbed separatrix into helical invariant manifolds referred to as the 'lobe structure' of the magnetic field lines [22]. ELM suppression can be expected by the formation of the lobe structure near the divertor region since the stochasticity and the radial transport of magnetic field lines arise from the exchange of magnetic flux through the lobes [17]. Plasma particles, moreover, move along the lobe field lines, and the edge plasma density is then expected to be sufficiently reduced to lead to ELM suppression. The lobe structure produced by separatrix splitting can cause the heat and power distributions to scatter onto the divertor plate with reduced peak loads at the striking points, and as a result, the divertor lifetime can be extended [22].

Figure 10 illustrates the lobe structures for even and odd parities in the hybrid operation scenario, respectively. For even parity, although the stochastic layer appears far from the top of the pedestal, the overlap of magnetic islands near the far edge region makes the lobe structure. However, ELMs would not be suppressed because the stochasticity of this lobe structure is not sufficient. On the other hand, for odd parity, the stochastic layer and the lobe structure appear more deeply inside the plasma edge region, which is expected to increase particle transport to cause the reduction in plasma density and pressure. In both parities, the scattering of peak heat load and the resultant lifetime extension of the divertor are expected by the existence of lobe structures. It is, therefore, anticipated that even if ELMs are not suppressed, RMP can be used to prolong the divertor lifetime. In addition, the lobe structure corresponds to the creation of a localized heat load pattern on the divertor plate. Pumping out the density during RMP application can make the heat removal by the divertor plate more difficult due to low density. Since the reduction in heat load on the divertor plate depends on the pedestal electron collisionality [23], more rigorous modeling and experiments will be required to verify the heat removal on the divertor plate and the extension of the divertor lifetime in various collisionality cases. The subject of heat flux spreading by lobe structures is an area of active research and there is still much to be learned about some key physics involved. The validity of the results obtained in this numerical work based on vacuum calculation will be verified by

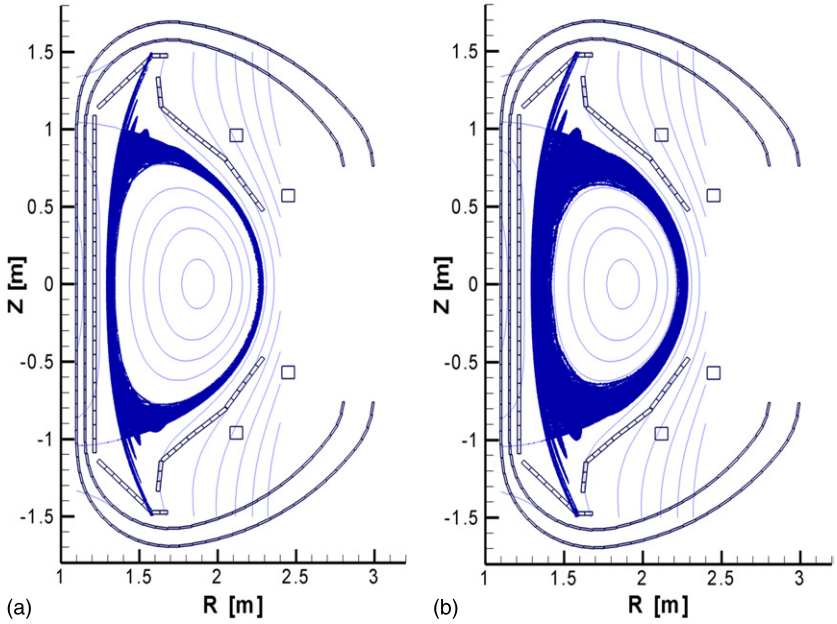

Figure 10. Lobe structures of magnetic fields found in the divertor region (*a*) for even parity and (*b*) for odd parity in the KSTAR hybrid operation scenario. The lobe structure for odd parity is distributed more deeply inside the divertor region compared with that for even parity, but the scattering of heat and particle fluxes on the divertor plate can be expected for both parities. By comparing the lobe structures and the positions of stochastic layers between the two parity cases, it is anticipated that ELMs can be more effectively suppressed by RMP in the odd parity case.

an extended modeling that considers plasma responses to RMP like rotational screening and by the future KSTAR experiments on the diverter D_α or IR camera measurements of density or heat pump-up onto the divertor plate.

4. Conclusion

The feasibility of RMP application to the KSTAR tokamak has been studied in this paper by estimating magnetic island configurations and sizes, resonant normal fields and Chirikov parameters for the steady-state and hybrid operation scenarios. The FEC control coils among the IVCCs in KSTAR are considered in this numerical work for the RMP analysis. The direction of current in each coil determines the toroidal mode number n and the parity (even or odd) under a fixed current of 10 kA in each coil. From this numerical simulation, stochastic magnetic field lines are expected to be formed when the external magnetic fields induced by the FEC coils in KSTAR are superposed to the equilibrium confinement fields.

When the external magnetic fields are produced by the $n = 2$ FEC coil currents, the magnetic islands and stochastic field lines for even and odd parities are observed in both the scenarios. Since the resonance of externally perturbed fields with equilibrium magnetic fields is affected by the parity of the FEC coil currents, the magnetic islands have distinctive configurations depending on the parity. In the steady-state operation, even parity is more effective in making the magnetic islands become stochastic field lines, while odd parity is better for the hybrid operation. The level of resonance, estimated by comparing the resonant normal fields with the pitch of the equilibrium magnetic fields, determines the size of magnetic islands.

A strong resonance enlarges the width of the magnetic islands so that the magnetic islands are overlapped in the edge plasma region for even parity in the steady-state scenario, but for odd parity in the hybrid scenario. The overlap of the islands and the formation of the stochastic layer are verified by the Chirikov parameter. For both operation scenarios, the Chirikov parameter is greater than unity near the pedestal top position implying that ELM suppression is possible in the KSTAR tokamak. The Chirikov parameter can give basic information on the current requirement of FEC power supply. The required currents to satisfy the vacuum criterion are about 12 kA and 10 kA for the steady-state and hybrid operation scenarios, respectively. These current requirements are realizable within a power supply limit of 15 kA in preparation for the FEC coils in KSTAR.

In addition, the stochastic field lines produce lobe structures for both parities in the hybrid operation scenario. For odd parity, the lobe structure of the stochastic magnetic field lines is formed in a proper edge region extended to the divertor region so that ELMs could be suppressed. The lobe structure formed for even parity is located far from the pedestal region so that ELM suppression is not expected. The lobe structure is also related to the divertor lifetime. Even though RMP cannot directly suppress ELMs, the lobe structure resulting from the RMP can be used for prolonging the divertor lifetime by splitting the heat and particle fluxes of the striking points on the divertor plate. Regardless of the feasibility of ELM suppression, the reduction in peak heat load on the divertor plate is expected to be effective for both even and odd parities.

Although the Chirikov parameters and the stochastic layer positions turn out to be favorable to the RMP ELM suppression from this work based on the vacuum superposition of magnetic fields, a more refined modeling including the effects of plasma responses should be considered for RMP application to the KSTAR tokamak as a method of ELM suppression. The future study will help in making the simulation results obtained from this work more convincing, and will be able to give further reliable information on the FEC coil's capability of ELM suppression in KSTAR operations.

Acknowledgments

The authors would like to thank Dr T E Evans of General Atomics (GA) in USA for his helpful comments on the heat flux spreading by lobe structures at low and high collisionality to value the results of this paper. This research was supported by the National R&D Program through the National Research Foundation of Korea (NRF) funded by the Ministry of Education, Science and Technology (2009-0082634).

References

[1] Na Y S, Kessel C E, Park J M, Yi S, Becoulet A, Sips A C C and Kim J Y 2009 *Nucl. Fusion* **49** 115018
[2] Evans T E *et al* 2008 *Nucl. Fusion* **48** 024002
[3] Lang P T *et al* 2004 *Nucl. Fusion* **44** 665–77
[4] Ongena J *et al* 2001 *Plasma Phys. Control. Fusion* **43** A11
[5] Bécoulet M *et al* 2003 *Plasma Phys. Control. Fusion* **45** A93
[6] Nardon E *et al* 2007 *J. Nucl. Mater.* **363–365** 1071–5
[7] Hawryluk R J *et al* 2009 *Nucl. Fusion* **49** 065012
[8] Evans T E, Joseph I, Moyer R A, Fenstermacher M E, Lasnier C J and Yan L W 2007 *J. Nucl. Mater.* **363–365** 570–4
[9] Joseph I *et al* 2008 *Nucl. Fusion* **48** 045009
[10] Bécoulet M *et al* 2008 *Nucl. Fusion* **48** 024003
[11] Canik J M *et al* 2010 *Phys. Rev. Lett.* **104** 045001
[12] Nardon E *et al* 2009 *Plasma Phys. Control. Fusion* **51** 124010

[13] Liang Y *et al* 2007 *Phys. Rev. Lett.* **98** 265004
[14] Lee G S *et al* 2000 *Nucl. Fusion* **40** 575–82
[15] Kim H K, Yang H L, Kim G H, Kim J Y, Jhang H, Bak J S and Lee G S 2009 *Fusion Eng. Des.* **84** 1029–32
[16] Wesson J 2004 *Tokamaks* 3rd edn, ed J Birman *et al* (New York: Oxford University Press) pp 108–9
[17] Evans T E, Roeder R K W, Carter J A, Rapoport B I, Fenstermacher M E and Lasnier C J 2005 *J. Phys.: Conf. Ser.* **7** 174
[18] Schaffer M J, Menard J E, Aldan M P, Bialek J M, Evans T E and Moyer R A 2008 *Nucl. Fusion* **48** 024004
[19] Park J K, Boozer A H and Menard J E 2008 *Phys. Plasmas* **15** 064501
[20] Evans T E, Moyer R A and Monat P 2002 *Phys. Plasmas* **9** 4957
[21] Na Y S and Kim J Y 2007 *Comput. Phys. Commun.* **177** 134
[22] Evans T E, Yu J H, Jakubowski M W, Schmitz O, Watkins J G and Moyer R A 2009 *J. Nucl. Mater.* **390–391** 789–92
[23] Jakubowski M W *et al* 2009 *Nucl. Fusion* **49** 095013